A protease-activated, near-infrared fluorescent probe for early endoscopic detection of premalignant gastrointestinal lesions

Joshua J. Yim[a,1], Stefan Harmsen[b,c,1], Krzysztof Flisikowski[d], Tatiana Flisikowska[d], Hong Namkoong[e], Megan Garland[f], Nynke S. van den Berg[g], José G. Vilches-Moure[h], Angelika Schnieke[d], Dieter Saur[i,j,k], Sarah Glasl[l,m], Dimitris Gorpas[l,m], Aida Habtezion[e], Vasilis Ntziachristos[l,m], Christopher H. Contag[n], Sanjiv S. Gambhir[b,o,p,q,2], Matthew Bogyo[a,r,s,3], and Stephan Rogalla[b,e,3]

[a]Department of Chemical and Systems Biology, Stanford University School of Medicine, Stanford, CA 94305; [b]Department of Radiology, Bio-X Program and Molecular Imaging Program, Stanford University School of Medicine, Stanford, CA 94305; [c]Department of Radiology, Perelman School of Medicine, University of Pennsylvania, Philadelphia, PA 19104; [d]Chair of Livestock Biotechnology, Technische Universität München, 85354 Freising, Germany; [e]Department of Medicine, Division of Gastroenterology & Hepatology, Stanford University School of Medicine, Stanford, CA 94305; [f]Department of Cancer Biology, Stanford University School of Medicine, Stanford, CA 94305; [g]Department of Otolaryngology–Head and Neck Surgery, Stanford University School of Medicine, Stanford, CA 94305; [h]Department of Comparative Medicine, Stanford School of Medicine, Stanford, CA 94305; [l]Division of Translational Cancer Research, German Cancer Research Center and German Cancer Consortium, 69120 Heidelberg, Germany; [j]Chair of Translational Cancer Research and Institute for Experimental Cancer Therapy, Klinikum rechts der Isar, School of Medicine, Technische Universität München, 81675 Munich, Germany; [k]Department of Internal Medicine II, Klinikum rechts der Isar, Technische Universität München, 81675 Munich, Germany; [l]Helmholtz Zentrum München, German Research Center for Environmental Health, Institute of Biological and Medical Imaging, 85764 Neuherberg, Germany; [m]Chair of Biological Imaging, TranslaTUM, Technische Universität München, 81675 Munich, Germany; [n]Department of Biomedical Engineering, Institute for Quantitative Health Science and Engineering, Michigan State University, East Lansing, MI 48824; [o]Department of Bioengineering, Stanford University, Stanford, CA 94305; [p]Department of Materials Science & Engineering, Stanford University, Stanford, CA 94305; [q]Canary Center at Stanford for Early Cancer Detection, Palo Alto, CA 94304; [r]Department of Pathology, Stanford University School of Medicine, Stanford, CA 94305; and [s]Department of Microbiology and Immunology, Stanford University School of Medicine, Stanford, CA 94305

Fluorescence imaging is currently being actively developed for surgical guidance; however, it remains underutilized for diagnostic and endoscopic surveillance of incipient colorectal cancer in high-risk patients. Here we demonstrate the utility and potential for clinical translation of a fluorescently labeled cathepsin-activated chemical probe to highlight gastrointestinal lesions. This probe stays optically dark until it is activated by proteases produced by tumor-associated macrophages and accumulates within the lesions, enabling their detection using an endoscope outfitted with a fluorescence detector. We evaluated the probe in multiple murine models and a human-scale porcine model of gastrointestinal carcinogenesis. The probe provides fluorescence-guided surveillance of gastrointestinal lesions and augments histopathological analysis by highlighting areas of dysplasia as small as 400 µm, which were visibly discernible with significant tumor-to-background ratios, even in tissues with a background of severe inflammation and ulceration. Given these results, we anticipate that this probe will enable sensitive fluorescence-guided biopsies, even in the presence of highly inflamed colorectal tissue, which will improve early diagnosis to prevent gastrointestinal cancers.

early detection | fluorescence | endoscopy | activity-based probe | high-risk patients

Early detection is critical in improving survival of patients with colorectal cancer (CRC), one of the most common and lethal malignancies worldwide (1). Conventional high-resolution white-light endoscopy (WLE) remains the gold standard for detecting colorectal adenomas, the most clinically relevant CRC precursor lesions (2). Unfortunately, due to their subtle appearance, these precursor lesions are often missed during endoscopy. In particular, nonpedunculated or flat lesions, which tend to have a five-fold higher propensity of being malignant, are often missed during WLE (3). In patients with inflammatory bowel disease (IBD) or Lynch syndrome, detection is even more challenging because lesions are present on a background of inflamed or ulcerated mucosa, which significantly increases the miss-rate relative to bowel healthy individuals (4). Furthermore, since these patients are at higher risk for developing CRC, it is imperative that they undergo frequent surveillance endoscopies

and timely therapeutic intervention to prevent malignant transformation of dysplastic lesions. Efforts therefore have been directed at improving endoscopic detection of dysplastic lesions, including narrow-band imaging (NBI) where blue and green light are used to enhance the mucosal contrast, or chromoendoscopy (CE), where dyes (e.g., methylene blue or indigo carmine) are topically applied onto the luminal surface to improve contrast between (pre)malignant

Significance

Early detection by white-light endoscopy (WLE) is the key procedure used in clinical care to prevent colorectal cancer (CRC). In high-risk patients to develop CRC, like in inflammatory bowel disease, the miss-rate of dysplastic lesions is three times higher compared to healthy individuals. In this study we explored the use of a near-infrared probe with fluorescence endoscopy as an adjunct to WLE to highlight adenomas. We demonstrated in clinically relevant animal models of colorectal carcinogenesis and ulcerative colitis that our strategy enabled improved detection using near-infrared fluorescence-guided colonoscopy without interfering in the clinical workflow. Since combined near-infrared fluorescent/WLE systems are already being clinically translated, our approach could result in improving the adenoma detection rate during colonoscopy particularly in high-risk patients.

lesions and normal mucosa. So far, however, no significant benefit in improving adenoma detection rate has been reported for either NBI or CE over white-light endoscopy (5–9).

To address the current relatively high miss-rate, optical imaging agents have been developed that highlight clinically relevant lesions during endoscopic surveillance. For example, we recently demonstrated in animal models of colorectal carcinogenesis that optically active, near-infrared fluorescent (NIRF) nanoparticle-based contrast agents enable endoscopic detection of premalignant lesions following intravenous (i.v.) administration (10–12). While these nanoparticle-based agents demonstrated great promise, perceived (long-term) toxicity issues surrounding nanoparticle-based agents may generally limit their clinical translation (12). Molecularly targeted fluorophores have been developed. A c-MET–targeting peptide conjugated to a NIRF dye was shown to improve adenoma detection in humans. However, due to intrinsic expression of c-MET by normal mucosa, the tumor-to-background ratio (TBR) was relatively low (maximum TBR = 1.51) (13).

In the current study, we evaluated a cathepsin protease-activatable probe for fluorescence-guided endoscopy. This probe, 6QC-ICG, consists of a near-infrared dye (ICG) that is coupled to an optical quencher (QC-1) via a peptidic substrate that is effectively cleaved by multiple cysteine cathepsins (Fig. 1). Because these proteases are overexpressed by tumor-associated macrophages (TAM) that infiltrate the colorectal tumor microenvironment, their activity is an ideal biomarker for cancer as well as various types of pathogenic inflammation (14, 15). Here we demonstrate that 6QC-ICG is an effective contrast agent that enables endoscopic detection of adenomas with high signal-to-background ratios in small animal models, a human-scale spontaneous large animal model, and in a mouse model of inflammation-induced colorectal carcinogenesis. We were also able to detect cancerous lesions in tissues in a model with a high background of inflammation, suggesting that the contrast generated by the probe is sufficient for clinical applications, where existing WLE has a high false-negative rate. Together, these data provide strong support for use of 6QC-ICG and other optical contrast agents to enhance endoscopic detection of cancer in the clinic.

Results

Detection of Intestinal Lesions in $Apc^{min/+}$ Mouse Model of Colorectal Carcinogenesis.

We first evaluated the 6QC-ICG probe for its ability to highlight relevant lesions in a mouse model of colorectal carcinogenesis. We chose the $Apc^{min/+}$ model because it accurately mimics the disease progression in humans with the spontaneous formation of predominantly intestinal adenomas at about 12 to 16 wk of age. As shown in Fig. 2A and *SI Appendix*, Fig. S1, polyps and lymph were highlighted along the entire small intestine, consistent with previous studies in this model (10, 11). Swiss roll analysis of the small intestine showed good correspondence between pathological analysis of the hematoxylin and eosin (H&E)-stained slides and NIRF imaging of the tissue block (Fig. 2 A and B). Overall, adenomas demonstrated a mean fluorescence signal of 3.0 ± 0.77 AU corresponding to a mean TBR of 3.9. The lymphatic tissue showed an average fluorescent signal of 3.00 ± 0.22 AU, which was significantly higher than background ($P < 0.0001$) and similar to the signal from the tumor tissue. (Fig. 2C).

Endoscopic Detection of Colorectal Lesions in $Apc^{Pirc/+}$ Rat Model of Colon Carcinogenesis.

We next tested the performance of 6QC-ICG in the $Apc^{Pirc/+}$ rat model because this larger animal model allowed us to evaluate the performance of the probe during real-time endoscopic colorectal surveillance. In contrast to the $Apc^{min/+}$ mice, which mainly develop intestinal adenomas, the $Apc^{Pirc/+}$ rats develop polypoid lesions in their colons (16–18). Moreover, $Apc^{Pirc/+}$ rats exhibit sex-specific cancer formation in males, similar to human colon carcinogenesis (16). Male rats were i.v. injected with 6QC-ICG at a dose of 1.15 mg/kg, which was allometrically scaled from the mouse dose of 2.3 mg/kg (19). After 12 to 18 h, anesthetized animals underwent an endoscopy by a trained gastroenterologist using our previously reported dual modal white-light (WL)/NIRF endoscopy system (11). As shown in Fig. 3A, NIRF highlighted the polyps during WL/NIRF endoscopy (Movie S1). To further validate the ability of 6QC-ICG to highlight colorectal adenomatous polyps, the animals were euthanized immediately after endoscopic surveillance, and colon tissues were collected for ex vivo analysis. Wide-field NIRF imaging of the freshly resected colons revealed hotspots that were confirmed to be adenomatous polyps by H&E histopathology analysis (Fig. 3 B and C). CD68 staining for macrophages also confirmed that fluorescence activity in tissue is consistent with increased CD68$^+$ macrophage presence (Fig. 3C). This analysis further demonstrated that adenomas as small as 2.0 mm, which were otherwise missed during gross visual inspection by a trained veterinarian pathologist, were highlighted by the increased fluorescent signal relative to normal tissue. Quantification of wide-field NIRF signal of the tumor versus normal tissue resulted in a mean TBR of 2.1 ± 0.30.

Evaluation of NIRF-Guided Endoscopy in the $APC^{1311/+}$ Porcine Model Using 6QC-ICG.

The porcine $APC^{1311/+}$ mutation is orthologous to a human mutation (APC^{1309}) responsible for a severe form of the inherited disorder familial adenomatous polyposis, and pigs carrying this mutation develop high-grade dysplastic colorectal adenomas (20, 21). Furthermore, these pigs are of similar size and weight to humans and allow use of standard clinical endoscopy equipment. Thus, it is an ideal model to further test the
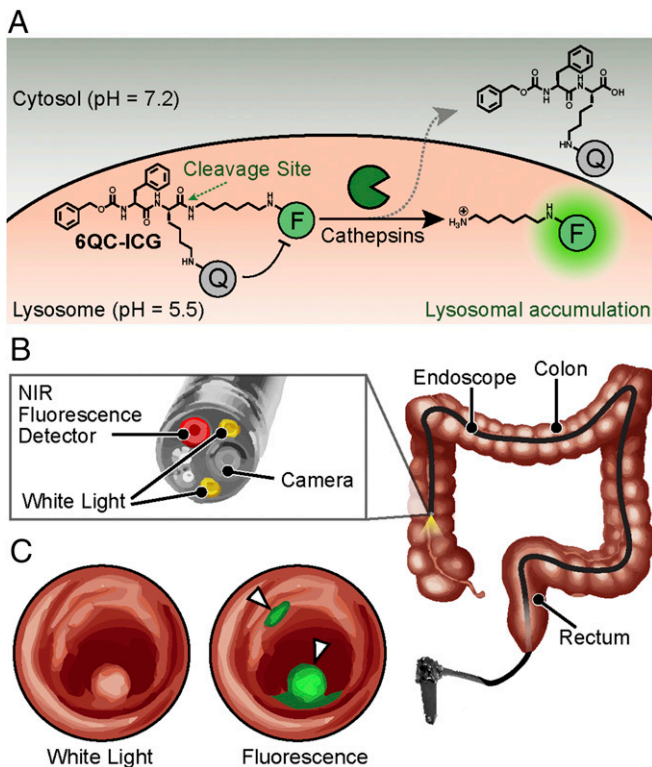
Fig. 1. Concept of fluorescence-guided detection of colorectal cancer using 6QC-ICG. (A) Chemical structure and schematic of the 6QC-ICG mechanism. (B) Schematic of a near-infrared (NIR) fluorescence endoscope used in the clinic. The probe is injected intravenously, and the GI physician uses an endoscope outfitted with an NIR (805/835 nm) detector and overlay fluorescence signals with a white-light image to detect lesion(s). (C) Sample image illustrating the concept of how our targeted fluorescent dye 6QC-ICG enables fluorescence-guided endoscopy of highlighted cancerous lesions that express cathepsins. Fluorescence is concentrated to the colorectal lesions and overlaid onto the white-light image.
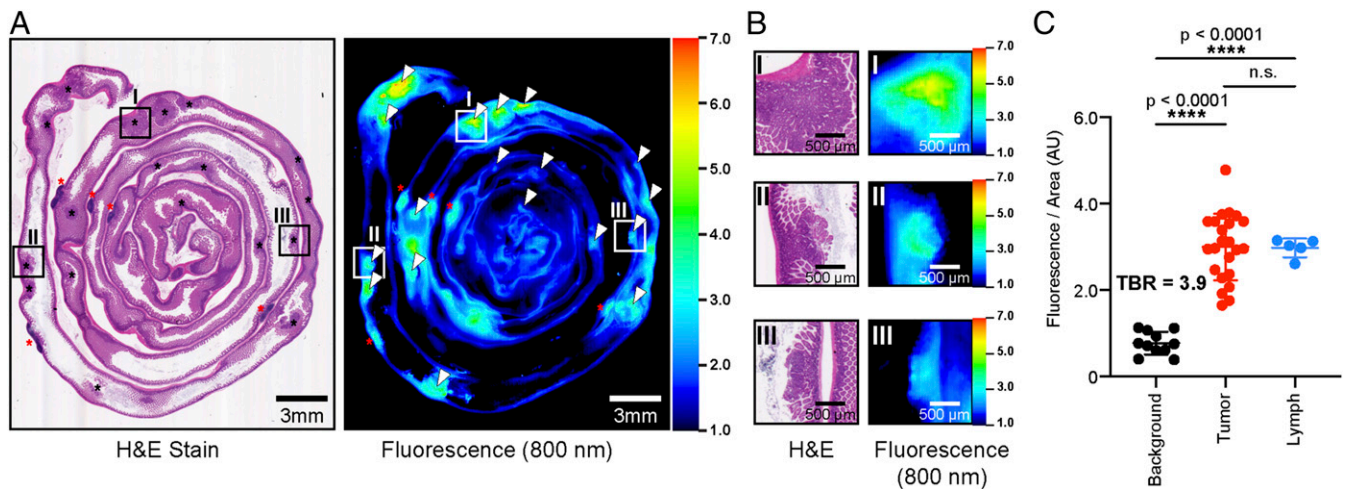
Fig. 2. NIRF Imaging of colorectal carcinogenesis in *Apc^min/+* mice using 6QC-ICG. (*A*) H&E and NIRF imaging of tissue block of small intestine tissue sections of a 12- to 16-wk-old *Apc^min/+* mouse injected with 6QC-ICG (euthanized 14 h post infection [PI], 2.3 mg/kg). Black asterisks denote tumors; red asterisks denote lymphatic tissue. White arrowheads in NIRF image correspond to black asterisks in H&E slide. Roman numerals indicate regions that are magnified and shown in *B*. (*B*) Zoomed-in images of H&E and corresponding 800-nm fluorescence scan of tissue block. (*C*) Tumors and gut-associated lymph tissues (lymph) demonstrate significantly higher NIRF signals relative to normal tissue (background). Error bars represent SDs. See *SI Appendix*, Fig. S1, for NIRF imaging of single 5-μm H&E-stained tissue section.

potential for application of the 6QC-ICG probe for use in fluorescence endoscopy. Two *APC^1311/+* male pigs were injected with either 0.25 or 1.0 mg/kg of 6QC-ICG probe i.v. 18 h prior to endoscopic surveillance. Combined WL/NIRF-guided endoscopy was conducted on both pigs, and, as shown in Fig. 4*A*, polyps were highlighted by 6QC-ICG (Movie S2). We performed an NIRF-guided biopsy on four NIRF-positive polyps and on a NIRF-negative area. Prior to sending the biopsied tissues to pathology, we performed wide-field NIRF imaging which confirmed the in vivo findings (i.e., four NIRF positive tissues and one NIRF-negative tissue specimen) (Fig. 4*B*). As validated by histopathological assessment of the biopsies, low-fluorescence signal (TBR < 1.2) corresponded to normal tissue (Fig. 4*B*) and high-fluorescence signal (TBR > 2.1) corresponded to the presence of dysplasia. The colon tissues from the pigs were analyzed ex vivo and showed a TBR ranging from 1.6 to 2.7 when imaged on the wide-field NIRF imager (Fig. 4*C*). Quantification of the fluorescence signals from the wide-field NIRF imager showed that at both the 0.25 and 1.0 mg/kg doses of 6QC-ICG, tumor tissue contained significantly higher fluorescence (*P* = <0.0001) than healthy background tissue (Fig. 4*D* and *SI Appendix*, Fig. S2D). Hotspots were easily identifiable even at a TBR of 1.6, and pathology analysis of the fluorescent hotspots confirmed dysplasia as noted by an independent veterinary pathologist using the H&E-stained slides (Fig. 4*E*). Direct NIRF scanning of the corresponding H&E slides showed fluorescence signals that overlap with the pathological annotation of the H&E (Fig. 4*E*). This analysis confirmed the detection of lesions as small as 400 μm using fluorescence imaging. Likewise, when these fluorescent tumor tissue sections were stained with H&E and scanned on the flatbed NIRF imager and signals were quantified, tumor tissue contained significantly higher fluorescence signals compared to healthy and lymph-derived tissues for both tested doses of probe (Fig. 4*F* and *SI Appendix*, Fig. S2E). The scanned slides showed a mean TBR of 2.5 ± 0.4 (1.0 mg/kg, Fig. 4*F*) and mean TBR of 1.30 ± 0.3 (0.25 mg/kg, *SI Appendix*, Fig. S2E). As shown in Fig. 4*D* and *SI Appendix*, Fig. S2C, although the mean fluorescence intensity values from the wide-field imaging of the tissue were roughly eight times higher at the 1.0 mg/kg dose than at the 0.25 mg/kg dose, the TBRs were similar for 1.0 mg/kg (TBR = 2.1) and 0.25 mg/kg (TBR = 2.3). While the raw fluorescence values from the wide-field imaging of the tissue were higher at the
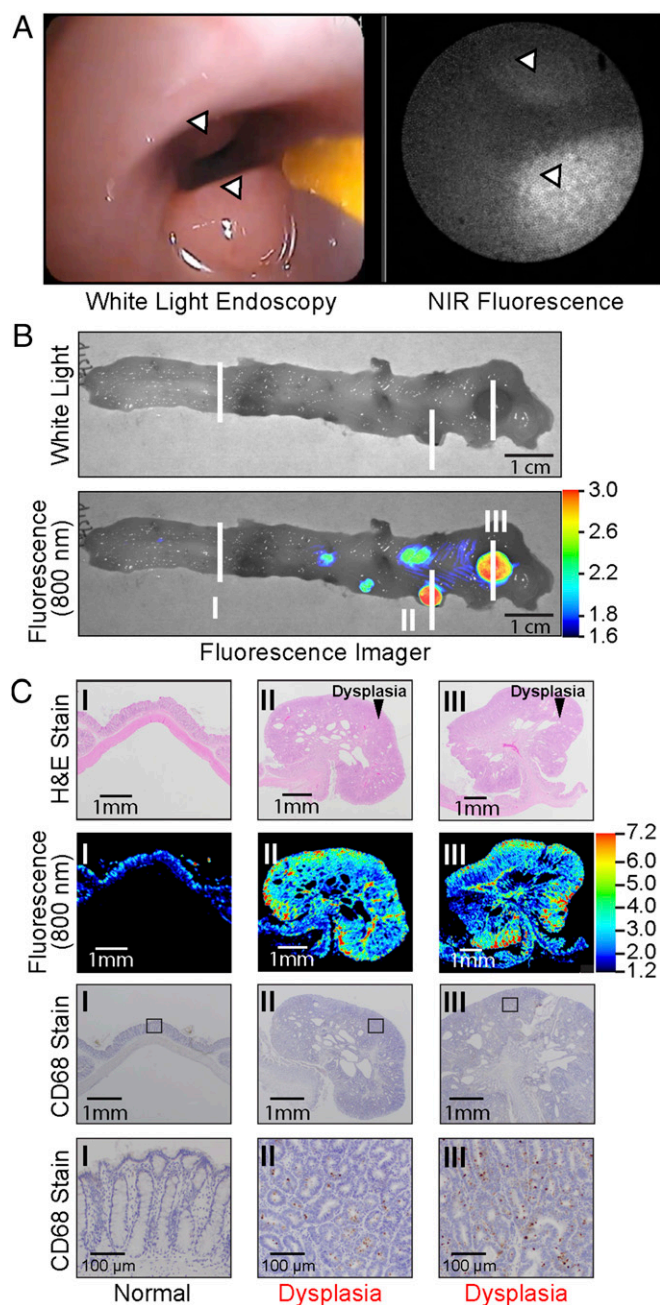
1.0 mg/kg dose than the 0.25 mg/kg dose, the TBRs were similar for 1.0 mg/kg (TBR = 1.87 ± 0.5) and 0.25 mg/kg (TBR = 1.90 ± 0.4) (*SI Appendix*, Fig. S2F). The calculated sensitivity, specificity, and precision were calculated to be 100% given no false negatives and no false positives in the group of 1.0 mg/kg. In the lower dose group of 0.25 mg/kg, both the precision and sensitivity were determined to be 93.3% with 80% specificity (*SI Appendix*, Fig. S3).

Evaluating 6QC-ICG in a Combined Model of GPR15 Knockout and Azoxymethane-Dextran Sulfate Sodium Mouse Model of Inflammation-Induced Carcinogenesis. To evaluate the 6QC-ICG probe in the context of severe inflammation and ulceration that occurs in IBD, we used a combination of the established chemically induced azoxymethane-dextran sulfate sodium (AOM-DSS) model described by Neufert et al. (22) and GPR15 het mice (23, 24). The GPR15 receptor controls specific homing of T cells in the colonic lamina propria, and a deficiency of this receptor causes severe colonic inflammation in mice starting at 10 wk (24). Combining this genetic background with the established protocol for induction of chemical colitis using AOM and proinflammatory DSS leads to an exacerbated response and increased polyp formation in the background of severe inflammation (22). We monitored the animals with WL endoscopy, and once polyps were visible by week 10 to 12, we injected the animals with 6QC-ICG (2.3 mg/kg i.v.). As shown in Fig. 5, the fluorescence signals corresponded to the dysplastic polypoid lesions as validated by H&E (Fig. 5 B and C). The fluorescent signals enabled guided detection of lesions even after fixation and H&E staining (Fig. 5C). The mean signal of the polyps produced a TBR of 1.81 ± 0.5 over healthy and lymphatic tissue, which, while lower than the values observed in the other models, still remains significant (P = 0.0011) over background and suggests that the probe could be effective in patients with high overall inflammation (Fig. 5D). Sensitivity, specificity, and precision were calculated to be 100% each in a postmortem autopsy. No false negatives or false positives were found (*SI Appendix*, Fig. S3).

Discussion

We evaluated a cathepsin-activated fluorescent substrate probe, 6QC-ICG, in combination with a NIRF/WL endoscopy, to improve early detection of dysplastic and early malignant lesions for high-risk patients. The probe was evaluated in well-established

Yim et al.
A protease-activated, near-infrared fluorescent probe for early endoscopic detection of premalignant gastrointestinal lesions

PNAS | 3 of 8
https://doi.org/10.1073/pnas.2008072118

Fig. 3. 6QC-ICG highlights adenomas during endoscopic surveillance in *Apc^Pirc/+* rats. (*A*) Polyps (arrowheads) in the colon of an *Apc^Pirc/+* rat are highlighted by 6QC-ICG during WL/NIRF endoscopy. (*B*) Wide-field NIRF imaging system of freshly resected colorectal tissue of an *Apc^Pirc/+* rat injected with 6QC-ICG. White lines and roman numerals indicate regions sampled for histology in *C*. (*C*) H&E histology, NIRF, and CD68 stain images of corresponding tissue sections (*B*, lesions I to III). The square indicates the location used for the higher-magnification (10×) microscopy images (*Bottom*).

mouse and rat models of carcinogenesis, a human-scale pig model of carcinogenesis, and a murine colitis model. We show that 6QC-ICG is able to highlight and distinguish colorectal adenomas in these animal models of colorectal carcinogenesis with the limit of detections of 400-μM small lesions that are clinically relevant to human health. We demonstrate that 6QC-ICG can be used not only for fluorescence-guided colonoscopic surveillance and decision making, but also for histopathological analyses of excised tissue using widely available NIRF imaging systems.

Many of the probes that are currently being evaluated for highlighting adenomas during NIRF-guided endoscopy are antibody-based probes (e.g., cetuximab-IRdye800CW, bevacizumab-IRdye800CW) (25, 26). While it was shown that on average these probes achieved a tumor-to-background ratio of ~1.8 (13, 26), a drawback of antibody-based imaging agents is their poor pharmacokinetic profile, which requires them to be administered i.v. 3 d prior to endoscopic examination (26). Furthermore, since only a single protein is targeted by antibody-based molecular-imaging agents, such probes are limited by receptor expression and heterogeneity of tumors. To compensate for tumor heterogeneity, efforts are being directed toward the use of multiple probes simultaneously, which has shown improvements for lesion detection (27). Unfortunately, using more than one targeting antibody increases the risk of adverse events and may cause additional regulatory hurdles for clinical use.

In contrast, the cathepsin protease-activated probe 6QC-ICG targets the tumor microenvironment, specifically, TAMs, and tumor cells themselves (28). This enables broad detection of the tumor microenvironments and accommodates all solid tumors, including those that present with heterogenous expression of tumor-associated receptors. Furthermore, since 6QC-ICG is a fluorescently quenched "smart probe" that turns on only when there is tumor-associated macrophage cathepsin activity, the probe is highly specific for colorectal tumors and does not produce fluorescent signals in normal mucosa, leading to improved tumor-to-background ratios. The postcleavage fluorescent product of 6QC-ICG accumulates within the lysosome of TAMs and allows for imaging without a wash-out period of the molecular dye enabling the endoscopist to immediately begin to examine the patient without having to perform time-consuming procedures in the endoscopy suite such as those required for chromoendoscopy after prior i.v. injection of the probe (29). Furthermore, since the fluorescence signal is activated only by cathepsins and is not active in the quenched form, there is no risk of nonspecific fluorescent signals due to dye contamination of instruments.
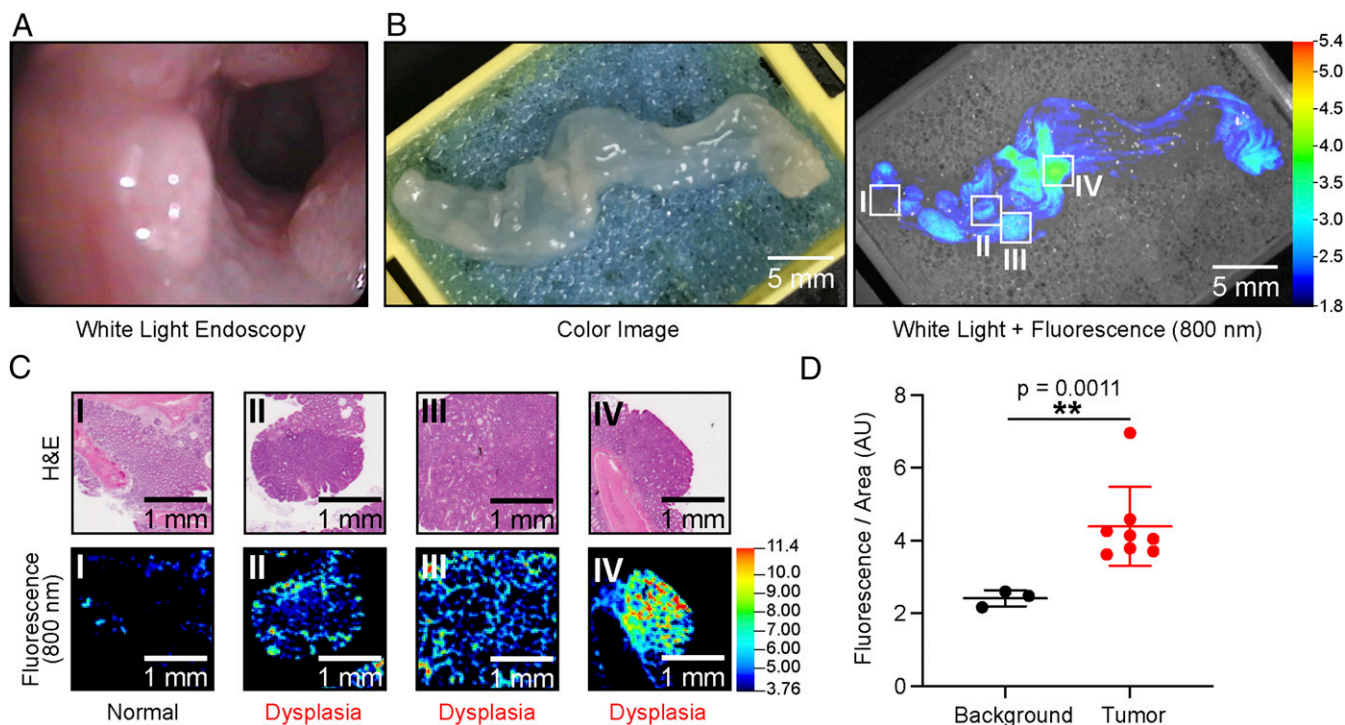
We tested the 6QC-ICG in established animal models of gastrointestinal (GI) carcinogenesis such as *Apc^min/+* mice, *Apc^Pirc/+* rats, and *APC^1311/+* pigs (16, 20, 21, 30, 31). These models spontaneously develop polypoid lesions similar to humans with familial adenomatous polyposis and thus are ideal models to study probe efficacy for detecting adenomas. We demonstrated that 6QC-ICG is able to highlight lesions during real-time colonoscopic surveillance 12 to 18 h post injection using a NIRF/WL-endoscopy system. Mean TBRs were 3.9 in murine, 2.1 in rat, and 2.5 in porcine models of carcinogenesis.

Histopathological examination of all highlighted lesions demonstrated that the majority of the detected lesions were adenomas. However, gut-associated lymphatic tissue and/or Peyer's patches, which contain macrophages, were also highlighted in these models, but demonstrated lower overall fluorescent signals. Furthermore, combined white-light/NIRF endoscopic imaging is performed parallel to the luminal surface (an ~145° to 180° angle) and not perpendicular as is the case with epifluorescence wide-field NIRF back table imaging. Consequently, mainly superficial mucosal lesions will be detected and not Peyer's patches, which are located in the deeper submucosal tissue layer.

In high-risk patients, such as those with ulcerative colitis, endoscopic surveillance plays a key role in preventing malignant transformation and early CRC detection. However, the false-negative rates for tumor detection in such high-risk patient cohorts remain higher than that of healthy individuals (4). Therefore, in addition to genetic models of carcinogenesis, we also evaluated the performance of our probe in an inflammation-induced colorectal carcinogenesis model that closely recapitulates ulcerative colitis (UC)-induced CRC (23). In this AOM-DSS mouse model, we showed that 6QC-ICG was able to highlight adenomatous lesions on a background of severe colonic inflammation. Even though the mean
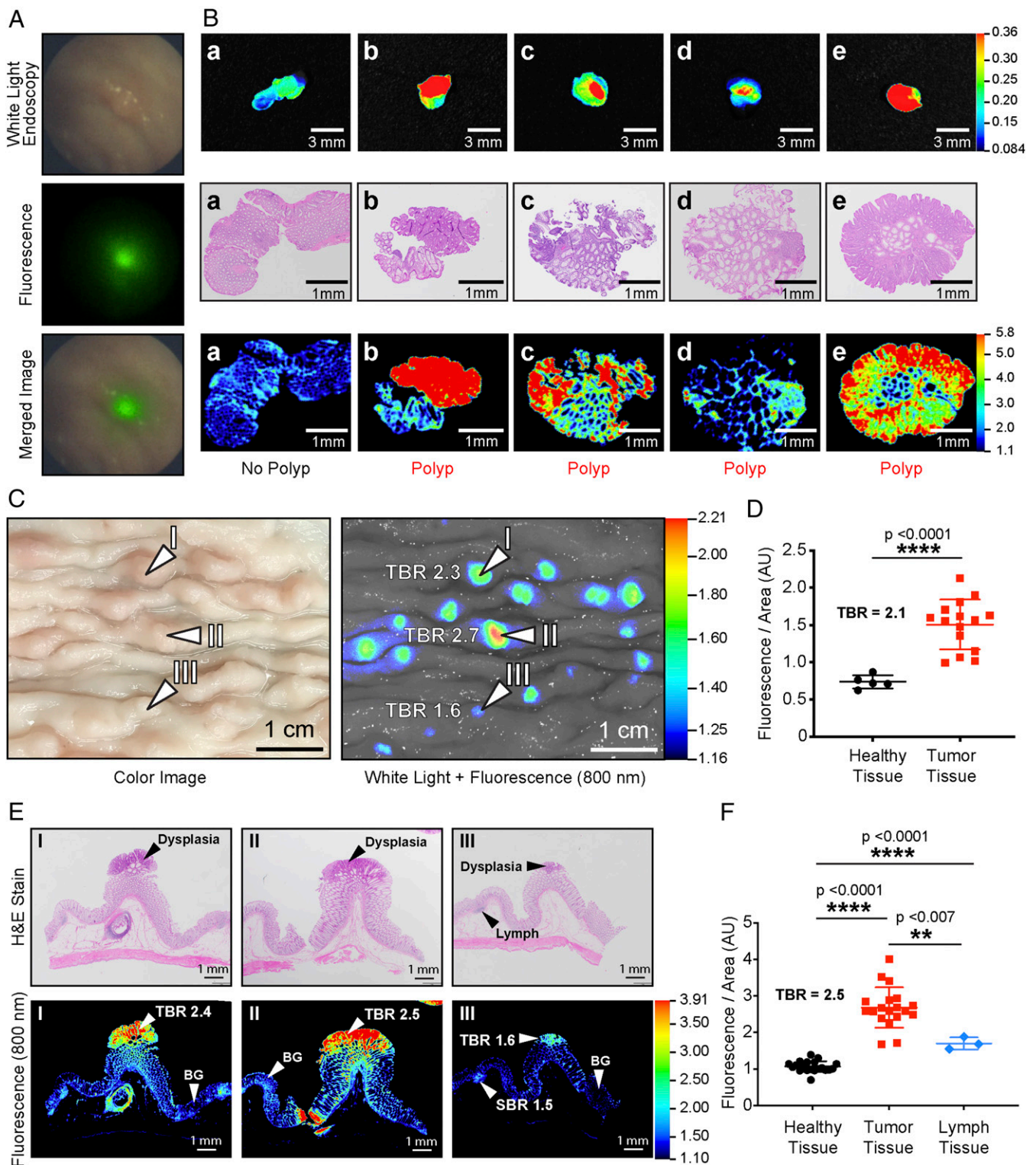
Fig. 4. NIRF-guided biopsy in porcine model of colorectal carcinogenesis. (*A*) NIRF-highlighted polyp in the colon of an *APC*[1311/+] pig (80 kg) after injection with 6QC-ICG (1.0 mg/kg). (*B*) (*Top* row) Wide-field NIRF images of tissues obtained during NIRF-guided biopsy. (*Middle* row) Corresponding H&E-stained tissue of biopsied tissue confirms the histological status of the tissues. (*C*) Images and tissue scans of colon tissue from an *APC*[1311/+] porcine model injected with 6QC-ICG (euthanized at 24 h PI, 1.0 mg/kg). Wide-field imaging with white light (*Left*) and corresponding 800-nm fluorescence image (*Right*). (*D*) Quantification of fluorescence of healthy and tumor tissues from wide-field imager for *APC*[1311/+] pigs injected with 1.0 mg/kg of probe. (*E*) Colon tissue slices stained with H&E (*Top*) and their corresponding flat-bed NIRF imager 800-nm scans (*Bottom*). (*F*) Quantification of fluorescence signals of healthy, tumor, and lymph sections of scanned colon tissues taken from the *APC*[1311/+] pigs injected with 1.0 mg/kg of probe. Error bars represent SDs.

Yim et al.
A protease-activated, near-infrared fluorescent probe for early endoscopic detection of premalignant gastrointestinal lesions

PNAS | 5 of 8
https://doi.org/10.1073/pnas.2008072118

Fig. 5. Imaging colorectal cancer injected with 6QC-ICG in AOM-DSS mice. (A) Screen capture of colon of an AOM-DSS–treated mouse in white-light endoscopy. (B) Images of colon tissue from an AOM-DSS mouse model injected with 6QC-ICG (euthanized 14 h PI, 2.3 mg/kg). Color image (*Left*) and white light + 800 nm fluorescence (*Right*). (C) H&E-stained slide images of corresponding tissue slices (*Top*) and flat-bed fluorescence scanner 800-nm scans of H&E-stained slides (*Bottom*). (D) Quantification of fluorescence signals of background and tumor sections of scanned colon tissue taken from AOM-DSS–treated mice (*n* = 5) (euthanized14 h PI, 2.3 mg/kg). Error bars represent SD.

TBR of 1.8 for the AOM-DSS mice was lower than that of the $Apc^{min/+}$ mice (TBR = 3.2), the signal was significantly brighter ($P = 0.0011$) than the signal of the inflamed tissue following 6QC-ICG administration. While it was challenging to distinguish adenomas from the inflamed tissue using white-light endoscopy (Fig. 5*A*), we were able to identify dysplastic lesions using fluorescence guidance (Fig. 5*B*). We envision that fluorescence-guided surveillance using 6QC-ICG in high-risk patients will improve the adenoma detection rate and allow physicians to prioritize certain sections of the colon for evaluation and biopsy.

While our studies showed that 6QC-ICG can highlight lesions in various models of colorectal carcinogenesis, clinical studies will be required to evaluate the efficacy and toxicity of our protease-activated imaging approach to identify colorectal dysplasia during routine colonoscopic surveillance, particularly in high-risk UC patients. The current clinical standard for UC involves the random collection of four biopsies every 10 cm along the length of the colon (32). Our NIRF-guided approach has the potential to be transformative for UC patients. By highlighting clinically significant lesions, 6QC-ICG enables targeted biopsy which will not only improve the adenoma detection rate but may also reduce the risk of injuries (e.g., perforation) due to unnecessary biopsy. Moreover, our approach will also contribute to reducing the time of colonoscopy procedures as well as the number of samples to be analyzed post procedure by pathology.

Overall, in the current study we demonstrate that the use of a protease-activated NIRF probe enables detection of clinically significant precursor lesions that may progress to CRC on a background of inflammation during real-time NIRF/WL colonoscopy. Our approach has been designed to be compatible with current clinical workflows. While we used a combined NIRF/WL endoscopy system that constituted clinically approved components, the development of commercial endoscopy systems with integrated NIRF/WL capabilities will contribute to the clinical translation of image-guided endoscopy and biopsy approaches. Ultimately, we believe that 6QC-ICG–mediated detection of clinically significant lesions during NIRF/WL endoscopy will contribute to prevention of CRC, particularly in high-risk patients such as seen in inflammatory bowel disease.

Materials and Methods

Synthesis of 6QC-ICG. Synthesis and characterization of 6QC-ICG was performed as previously outlined by Yim et al. (28). All reagents and materials used in the synthesis of 6QC-ICG were obtained from commercial sources and used without further purification. The *N*-hydroxysuccinimide (NHS) ester of IRDye QC-1 was purchased from LI-COR Biosciences, and ICG-NHS ester was purchased from Intrace Medical. Compounds were purified using reverse-phase preparative high-performance liquid chromatography. The 6QC-ICG was stored as a 10-mM stock solution in dimethyl sulfoxide (DMSO) and diluted in PBS at a concentration to achieve the appropriate dose following i.v. injection. Of note, the final DMSO concentration was kept below 1% (vol/vol).

Animal Models. In vivo studies using animal models at Stanford University were conducted in accordance with current NIH and Stanford University Institutional Animal Care and Use Committee (IACUC) guidelines (mouse and rat studies: APLAC #27715). Animals were under the direct oversight of an animal care and use program that was American Association for Accreditation of Laboratory Animal Care (AAALAC) International-accredited and Public Health Service (PHS) assured. In vivo studies in a porcine model were performed at the Technical University of Munich and approved by the Federal Government of Bavaria (ROB55.2–2-2532.Vet_02-18–33) and Stanford University (IACUC #30122).

Adenoma Detection in a Murine Model of Intestinal Polyposis. Heterozygous C57BL/6J-ApcMin ($Apc^{Min/+}$) female mice were obtained from the Jackson Laboratory and were raised on a high-fat diet (Teklad Global 2018 diet, Envigo), which contained 18% (wt/wt) protein, 6% (wt/wt) fat, moderate phytoestrogens, and no alfalfa. Based on previous studies, mice (14 to 20 wk old; *n* = 5) were i.v. injected with 6QC-ICG in PBS (dose 2.3 mg/kg) (28). After

Yim et al.
A protease-activated, near-infrared fluorescent probe for early endoscopic detection of premalignant gastrointestinal lesions

14 to 18 h, the animals were euthanized, and the small intestines were harvested, rinsed with PBS, and processed for formalin-fixed paraffin embedding and subsequent H&E tissue staining. Wide-field NIRF imaging was performed ($\lambda_{ex,em}$ 785 nm, >800 nm) on the paraffin-embedded tissue block prior to H&E tissue sectioning using a Pearl Trilogy Small Animal Imaging System (LI-COR Biosciences). Images were analyzed using Image Studio Software (LI-COR Biosciences). Individual 5-μm thick, H&E-stained tissue sections of the same block were imaged on an Odyssey CLx ($\lambda_{ex,em}$ 785 nm, >800 nm; 21-μm resolution; LI-COR Biosciences).

Endoscopic Detection of Adenomas in Apc$^{Pirc/+}$ Rats. Heterozygous Apc$^{Pirc/+}$ rats (12 to 16 wk old) were provided by James Amos-Landgraf, Department of Veterinary Pathobiology, University of Missouri, Columbia, MO, and were fed a Teklad Global 2018 diet (Envigo), which contains 18% (wt/wt) protein, 6% (wt/wt) fat, moderate phytoestrogens, and no alfalfa. The Apc$^{Pirc/+}$ rats (n = 5) were administered 6QC-ICG (1.15 mg/kg) via tail-vein injections. After 12 to 18 h, the animals were anesthetized with 2% (vol/vol) isoflurane (Fluriso, VetOne). Their colons were lavaged with a PBS enema. Endoscopy was performed with a white-light endoscope (Pentax EPK-1000 and G110074, Pentax) outfitted with a custom-built NIRF-imaging endoscopy system consisting of a Spyglass fiberscope (Boston Scientific), a 785-nm excitation laser operating at 10 mW, a long-pass edge filter (EdgeBasic, BLP01-785–25, Semrock), and an electron multiplying charge-coupled device (EMCCD) camera (Luca R, Andor Technology). Video-rate white-light and fluorescence imaging were recorded using GrabBee 2.0 (VideoHome Technology) and Solis (Andor Technology), respectively, and screen was captured with Captivate screen capturing software (Adobe). Following endoscopy, animals were euthanized via cervical dislocation. Intestines and colons of the rats were rinsed with PBS three times, and NIRF imaging was performed ($\lambda_{ex,em}$ 785 nm, >800 nm) on the freshly resected tissues. Next, the tissues were fixed in 10% neutral-buffered formalin and processed for histological examination.

Endoscopic Detection of Adenomas in Apc$^{1311/+}$ Pigs. Two APC$^{1311/+}$ pigs (16 to 20 mo old) weighing 66 and 82 kg received 6QC-ICG 0.25 and 1.0 mg/kg by i.v. administration. After 12 to 18 h, the animals were anesthetized by intramuscular (IM) injection of ketamine (20 mg/kg body weight) and azaperone (2 mg/kg body weight), and fluorescence-guided endoscopy was performed using a custom-built combined NIRF/WL endoscopy system equipped with a ViZaar fiberscope (A250L2000, viZaar Industrial Imaging) (33), a 780-nm laser operating at 70 mW/cm^2 at the fiberscope's distal end for NIRF imaging, and a 250-W halogen lamp (KL-2500 LCD, Schott) for color imaging. Fluorescence was detected through an 800-nm long-pass (FELH0800, Thorlabs) and an 810/90-nm bandpass (ET810/90, Chroma Technology) filter, while color imaging was filtered by a 665-nm shortpass filter (FF01-665/SP-25, Semrock). NIRF was detected with an EMCCD (DV897DCS-BV, Andor Technology), and color imaging was performed using a charge-coupled device (pixelfly qe, PCO). For the postmortem collection of samples, the pigs were sedated by IM administration of ketamine (20 mg/kg body weight) and azaperone (2 mg/kg body weight), rendered unconscious by a captive bolt gun applied to the forehead, and then exsanguinated. Samples of colorectal and muscle tissues were removed for analysis. Random samples of freshly resected colon and rectum tissues were cut into sections ~15 cm in length. All tissues were fixed in 10% neutral-buffered formalin. The formalin-fixed colorectal porcine tissues were imported from Germany to Stanford, CA, under a US Veterinary Permit for importation and transport of controlled materials and organisms and vectors (US Department of Agriculture Permit Number 136,396). Upon receipt, NIRF imaging was performed ($\lambda_{ex,em}$ 785 nm, >800 nm) on the formalin-fixed porcine colorectal tissues using the Pearl Trilogy Small Animal Imaging System (LI-COR Biosciences). Images were analyzed using Image Studio Software (LI-COR Biosciences).

Adenoma Detection in a Murine Model of Inflammation-Induced Colorectal Carcinogenesis. We adjusted the protocols from Neufert et al. (22) and Kim et al. (24) and chemically induced colitis and subsequent colonic polyps in a genetically modified mouse model (23). GPR15 Het mice (n = 5) were injected intraperitoneally with the procarcinogen AOM (10 mg/kg; Sigma-Aldrich). Seven days later, mice received drinking water containing 2% (wt/vol) DSS (MP Biomedicals; molecular weight: 36 to 50 kDa) for 7 d, followed by 14 d

of regular drinking water. The DSS administration was repeated for two more cycles.

Histopathology. Tissues fixed in 10% neutral-buffered formalin (4 °C overnight) were subsequently processed to be embedded in paraffin. Tissue sections (5 μm) were stained with H&E. CD68 staining of rat colon tissue samples was performed by Stanford's Comparative Medicine core facility using polyclonal CD68 antibodies (25757-1-AP; 1:200; Proteintech Group). All specimens were examined by two trained veterinary pathologists.

Region of Interest Calculations.
Apc$^{min/+}$ mouse model Swiss roll analysis. The tumor region of interest (ROI) was assigned by an independent veterinary pathologist to an H&E slide prior to fluorescence imaging. ROI area was then superimposed on fluorescence scan, and average fluorescence intensity (AU) was calculated using Image Studio Software (LI-COR Biosciences). Normal tissue ROI-selected from sections not marked as dysplasia or lymph tissue by pathologist and average fluorescence intensity (AU) was calculated in same manner as tumor ROI. Twenty-three tumor and 11 healthy tissue were ROI-selected from scan.
APC$^{1311/+}$ pig wide-field analysis. Tumor/dysplasia ROI was established by drawing a circular ROI of the set area around fluorescent hotspots of excised colon tissue, and fluorescence (AU) was calculated using Image Studio Software (LI-COR Biosciences). Normal tissue ROI was determined by drawing a circular ROI with an equivalent set area in nonfluorescent spots of colon tissue. Seventeen tumor and 3 healthy tissue ROIs were selected from animals injected with 1 mg/kg probe. Fifteen tumor and 5 healthy tissue ROIs were selected from animals injected with a 0.25 mg/kg probe.
APC1311/+ pig histology slide analysis. A tumor/dysplasia ROI independently was assigned by a veterinary pathologist on H&E slide. The ROI area was then superimposed on a fluorescence scan, and average fluorescence intensity (AU) was calculated using Image Studio Software (LI-COR Biosciences). Normal tissue ROI was selected from tissue sections not marked as dysplasia or lymph tissue by the pathologist, and average fluorescence intensity (AU) was calculated in same manner as tumor ROI. One tumor/dysplasia ROI, one background ROI, and one lymph ROI (when present) were selected for each slide.
GPR15 het AOM-DSS mouse model histology analysis. A tumor/dysplasia ROI was established by drawing the ROI area around fluorescent hotspots, and average fluorescence intensity (AU) calculated using Image Studio Software (LI-COR Biosciences). Normal tissue ROI was determined by drawing the ROI within nonfluorescent spots of colon tissue and calculating average fluorescence intensity (AU). Independently, a blinded pathologist confirmed whether ROI was tumor or healthy based on the H&E slide. Ten tumor and 3 healthy tissue ROIs were selected.

Statistical Analysis. All statistical analyses were performed in Excel (Microsoft) and Prism (Graphpad Software). The TBR was calculated by dividing the intensity of the ROI of the tumor by the ROI of normal tissue. All values in figures are presented as means ± SD unless otherwise noted in the text and figure legends. Statistical significance was calculated on the basis of the Student's t test (two-tailed, unpaired).

Data Availability. All study data are included in the article and supporting information.

1. S. Rogalla, C. H. Contag, Early cancer detection at the epithelial surface. *Cancer J.* **21**, 179–187 (2015).
2. I. A. Issa, M. Noureddine, Colorectal cancer screening: An updated review of the available options. *World J. Gastroenterol.* **23**, 5086–5096 (2017).
3. R. M. Soetikno et al., Prevalence of nonpolypoid (flat and depressed) colorectal neoplasms in asymptomatic and symptomatic adults. *JAMA* **299**, 1027–1035 (2008).
4. R. Soetikno et al., The detection of nonpolypoid (flat and depressed) colorectal neoplasms in patients with inflammatory bowel disease. *Gastroenterology* **144**, 1349–1352.e1–6 (2013).
5. A. Nagorni, G. Bjelakovic, B. Petrovic, Narrow band imaging versus conventional white light colonoscopy for the detection of colorectal polyps. *Cochrane Database Syst. Rev.* **1**, CD008361 (2012).

Yim et al.
A protease-activated, near-infrared fluorescent probe for early endoscopic detection of premalignant gastrointestinal lesions

6. L. Dinesen, T. J. Chua, A. J. Kaffes, Meta-analysis of narrow-band imaging versus conventional colonoscopy for adenoma detection. *Gastrointest. Endosc.* **75**, 604–611 (2012).

7. S. F. Pasha *et al.*, Comparison of the yield and miss rate of narrow band imaging and white light endoscopy in patients undergoing screening or surveillance colonoscopy: A meta-analysis. *Am. J. Gastroenterol.* **107**, 363–370, quiz 371 (2012).

8. L. C. Sabbagh, L. Reveiz, D. Aponte, S. de Aguiar, Narrow-band imaging does not improve detection of colorectal polyps when compared to conventional colonoscopy: A randomized controlled trial and meta-analysis of published studies. *BMC Gastroenterol.* **11**, 100 (2011).

9. R. Bisschops *et al.*, Chromoendoscopy versus narrow band imaging in UC: A prospective randomised controlled trial. *Gut* **67**, 1087–1094 (2018).

10. S. Harmsen *et al.*, Detection of premalignant gastrointestinal lesions using surface-enhanced resonance raman scattering-nanoparticle endoscopy. *ACS Nano* **13**, 1354–1364 (2019).

11. S. Rogalla *et al.*, Biodegradable fluorescent nanoparticles for endoscopic detection of colorectal carcinogenesis. *Adv. Funct. Mater.* **29**, 1904992 (2019).

12. I. S. Alam *et al.*, Emerging intraoperative imaging modalities to improve surgical precision. *Mol. Imaging Biol.* **20**, 705–715 (2018).

13. J. Burggraaf *et al.*, Detection of colorectal polyps in humans using an intravenously administered fluorescent peptide targeted against c-Met. *Nat. Med.* **21**, 955–961 (2015).

14. S. Sensarn *et al.*, A clinical wide-field fluorescence endoscopic device for molecular imaging demonstrating cathepsin protease activity in colon cancer. *Mol. Imaging Biol.* **18**, 820–829 (2016).

15. E. Barbera-Guillem, J. K. Nyhus, C. C. Wolford, C. R. Friece, J. W. Sampsel, Vascular endothelial growth factor secretion by tumor-infiltrating macrophages essentially supports tumor angiogenesis, and IgG immune complexes potentiate the process. *Cancer Res.* **62**, 7042–7049 (2002).

16. J. M. Amos-Landgraf *et al.*, A target-selected Apc-mutant rat kindred enhances the modeling of familial human colon cancer. *Proc. Natl. Acad. Sci. U.S.A.* **104**, 4036–4041 (2007).

17. R. van Boxtel, M. N. Gould, E. Cuppen, B. M. Smits, ENU mutagenesis to generate genetically modified rat models. *Methods Mol. Biol.* **597**, 151–167 (2010).

18. M. Oshima *et al.*, Loss of Apc heterozygosity and abnormal tissue building in nascent intestinal polyps in mice carrying a truncated Apc gene. *Proc. Natl. Acad. Sci. U.S.A.* **92**, 4482–4486 (1995).

19. A. B. Nair, S. Jacob, A simple practice guide for dose conversion between animals and human. *J. Basic Clin. Pharm.* **7**, 27–31 (2016).

20. T. Flisikowska *et al.*, A porcine model of familial adenomatous polyposis. *Gastroenterology* **143**, 1173–1175.e7 (2012).

21. T. Flisikowska *et al.*, Porcine familial adenomatous polyposis model enables systematic analysis of early events in adenoma progression. *Sci. Rep.* **7**, 6613 (2017).

22. C. Neufert, C. Becker, M. F. Neurath, An inducible mouse model of colon carcinogenesis for the analysis of sporadic and inflammation-driven tumor progression. *Nat. Protoc.* **2**, 1998–2004 (2007).

23. L. P. Nguyen *et al.*, Role and species-specific expression of colon T cell homing receptor GPR15 in colitis. *Nat. Immunol.* **16**, 207–213 (2015).

24. S. V. Kim *et al.*, GPR15-mediated homing controls immune homeostasis in the large intestine mucosa. *Science* **340**, 1456–1459 (2013).

25. J. J. Tjalma *et al.*, Molecular fluorescence endoscopy targeting vascular endothelial growth factor a for improved colorectal polyp detection. *J. Nucl. Med.* **57**, 480–485 (2016).

26. E. Hartmans *et al.*, Potential red-flag identification of colorectal adenomas with wide-field fluorescence molecular endoscopy. *Theranostics* **8**, 1458–1467 (2018).

27. W. S. Tummers *et al.*, Selection of optimal molecular targets for tumor-specific imaging in pancreatic ductal adenocarcinoma. *Oncotarget* **8**, 56816–56828 (2017).

28. J. J. Yim, M. Tholen, A. Klaassen, J. Sorger, M. Bogyo, Optimization of a protease activated probe for optical surgical navigation. *Mol. Pharm.* **15**, 750–758 (2018).

29. A. Rastogi, Clinical review: How to recognize subtle lesions in the colon. *ASGE Leading Edge* **5**, 1–13 (2015).

30. A. R. Moser *et al.*, ApcMin, a mutation in the murine Apc gene, predisposes to mammary carcinomas and focal alveolar hyperplasias. *Proc. Natl. Acad. Sci. U.S.A.* **90**, 8977–8981 (1993).

31. A. R. Moser, H. C. Pitot, W. F. Dove, A dominant mutation that predisposes to multiple intestinal neoplasia in the mouse. *Science* **247**, 322–324 (1990).

32. J. A. Eaden, J. F. Mayberry; British Society for Gastroenterology; Association of Coloproctology for Great Britain and Ireland, Guidelines for screening and surveillance of asymptomatic colorectal cancer in patients with inflammatory bowel disease. *Gut* **51** (suppl. 5), V10–V12 (2002).

33. J. Glatz *et al.*, Near-infrared fluorescence cholangiopancreatoscopy: Initial clinical feasibility results. *Gastrointest. Endosc.* **79**, 664–668 (2014).

Yim et al.
A protease-activated, near-infrared fluorescent probe for early endoscopic detection of premalignant gastrointestinal lesions